ear. MLAEFs from the right and left cerebral hemispheres were recorded separately. Simultaneously, AMLRs were recorded using surface electrodes placed at Cz (vertex), C3 (over the left temporal lobe) and C4 (over the right temporal lobe). The ground electrode was placed on the ear lobe of the stimulated ear. The recording bandwidth was 1–2000 Hz. The peak latency (milliseconds) and amplitude [root-mean-square (r.m.s.) value in the case of the MLAEF] were measured.

Equivalent current dipoles (ECDs) were estimated at 0.96-ms intervals based on the magnetic field data obtained at each measurement point. ECDs are a collection of hypothetical dipoles that would produce the pattern of the magnetic field recorded at a particular point in time. Each ECD is represented as a vector, i.e. having an origin and direction within the brain, and a strength. A correlation coefficient is calculated between the predicted field for each ECD and the actual magnetic field pattern. Among the ECDs at each latency, that with the highest correlation coefficient was selected as a Pam current source (hereafter ECD refers to the ECD with the highest correlation coefficient). ECDs were judged reliable when their correlation coefficients were >0.98, and brain MRI overlays were performed only for the reliable ECDs. The position of an ECD was represented in a coordinate system.

Brain MRI scans were obtained using an image scanner (Sharp JX-600) and transferred to a data analysis processor.

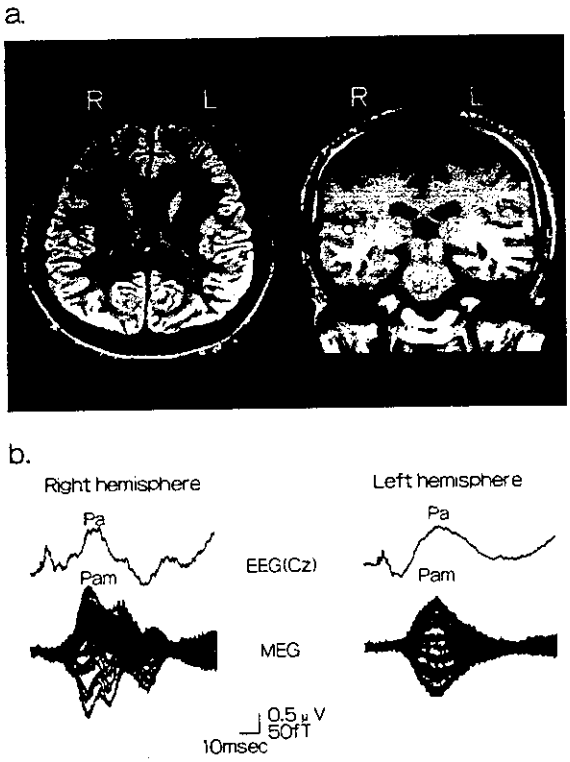

Fig. 1. (a) Superimposition of the ECD on the auditory cortex of the brain MRI scan. A white circle indicates the localization of the ECD. (b) Typical simultaneous recordings of AMLRs and MLAEFs in a normal subject, a 25-year-old male. Right- and left-hemisphere recordings were made with contralateral stimulation.

RESULTS

Controls

AMLRs and MLAEFs were recorded from 15 normal subjects for comparison. Typical recordings are shown in Fig. 1, in which the ECD is superimposed on the brain MRI scan. The ECD is localized in the auditory cortex in the right and left hemispheres. Control data are shown in Fig. 2a.

Patients

Left auditory cortex lesions. Nine patients who manifested sensory aphasia were studied. They were right-handed and had normal hearing. In most cases, their left primary and secondary auditory cortices had been damaged by their cerebrovascular accidents. Fig. 3 shows MLAEFs and the dipole localization fitted to the brain MRI scan for a typical patient, a 64-year-old male.

In Fig. 2b, the average latency and amplitude of the Pa in the AMLRs and the Pam in the MLAEFs from the right and left hemispheres are shown. There is no significant difference in the latency or amplitude of the Pa from the right and left hemispheres in the AMLRs. However, there is a significant difference in the r.m.s. amplitude of the Pam from the right and left hemispheres in MEG; there was no significant left–right difference in Pam latency.

Dipole locations of ECDs with relative coefficients >0.98 were calculated. For the right hemisphere, eight of nine patients had coefficients >0.98; only one of nine patients had no such correlation for the left hemisphere. Statistically, there was no difference between normal subjects and patients for the right hemisphere. A comparison between the left and right hemispheres among the patients, using paired t-tests, showed a significant difference in amplitude ($p<0.05$) in eight patients. The other patient, whose relative coefficient was >0.98, did not show significant differences between the right and left hemispheres.

Right auditory cortex lesion. Fig. 4 shows AMLRs and MLAEFs and the dipole localization fitted to the brain MRI scan for a typical patient, a 63-year-old male. The Pa of the AMLRs and MLAEFs was present from the left hemisphere in response to a right-ear stimulus. The Pam from the right hemisphere

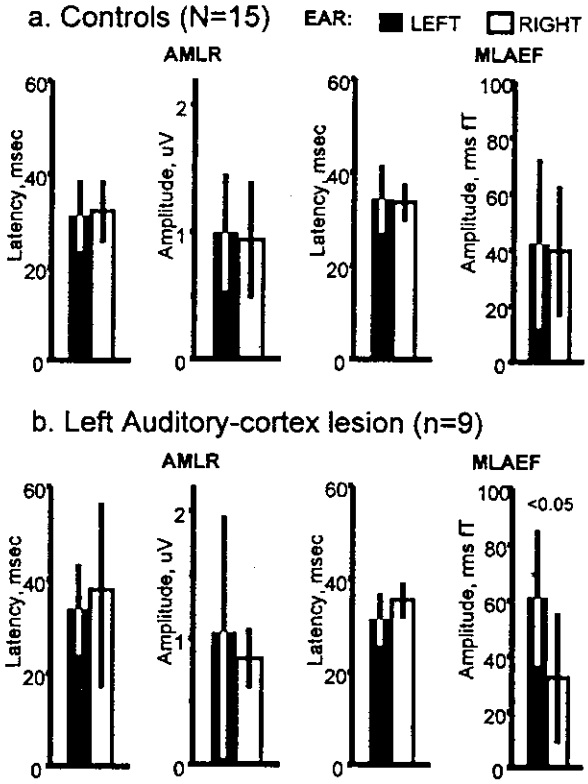

Fig. 2. (a) In data from 15 controls. there is no significant difference between the left and right hemispheres (right- and left-ear stimulation. respectively) in terms of the latency or amplitude of the AMLR or MLAEF. (b) In nine patients with left-hemisphere lesions. the MLAEF amplitude is significantly reduced for right-ear stimulation.

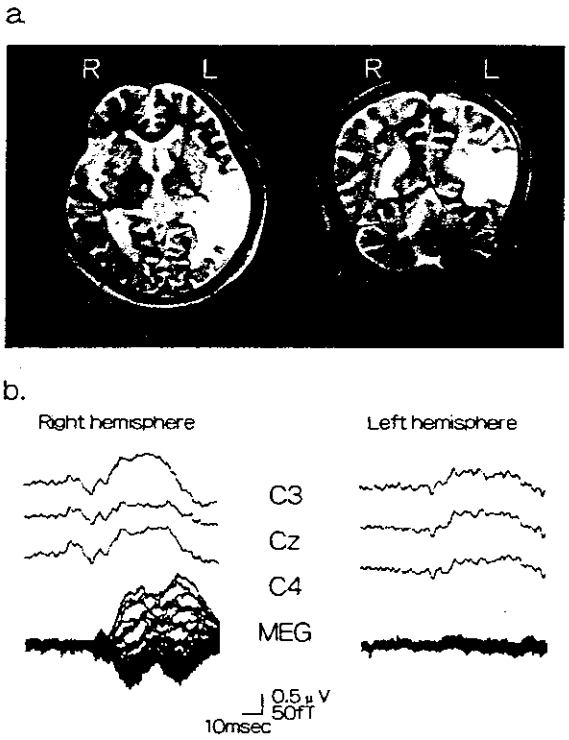

Fig. 3. A typical patient (64-year-old male) with a left auditory cortex lesion in the unilateral temporoparietal infarction. Brain MRI scans. AMLRs and MLAEFs are shown. The MLAEF is absent from the left hemisphere but is present from the right hemisphere. However. the AMLR persists bilaterally.

in response to a left stimulus was absent but the Pam from the left hemisphere was present in response to a right-ear stimulus. However. Pa of AMLR was present from both hemispheres.

DISCUSSION

This study demonstrates that the MLAEF generator is located in the auditory cortex because the ECD was localized to this area in patients with an undamaged auditory cortex but disappeared in patients with a damaged auditory cortex. The Pam of the MLAEF. which was evoked with the same latency as the Pa in the normal AMLR. was impaired or abolished in patients with lesions of the auditory cortex or its radiations. Pantev et al. (8) reported that clear Pam components of MLAEFs were recorded from the left hemisphere of each of 12 normal subjects when a short tone-burst stimulation was applied. As the specification of the SQUID gradiometers and the nature of the sound stimuli used differed between the studies. the results cannot be compared easily: however. the ECDs of the Pam were reported to be located in the left primary auditory cortex in the study of Pantev et al. (8). In our study. the ECDs recorded over the left hemisphere in normal subjects were localized in the primary auditory cortex. However. they were located slightly posterior to the estimated position reported by Pantev et al. (8) in normal subjects. This difference may be explained by recalling that the ECD is a hypothetical point source. which represents the center of activity (analogous to the center of gravity) of a source having some physical size. If the source includes both the anterior and posterior auditory cortices. an anterior lesion will cause the apparent center to move posteriorly. In our studies of the relationship between the damaged area and the position of the ECD. it is clear that most of the Pam disappears if the auditory cortex or auditory radiation is damaged. but that the Pam from the undamaged hemisphere persists. Our results suggest that at least part of the auditory cortex can be preserved. judging from the MLAEF analysis and the estimated position of the ECD.

For the reasons stated above. we conclude that the Pa and Pam do not reflect activities of identical generators. Woods et al. (4) speculated that the Pa amplitude is significantly influenced by the gradual

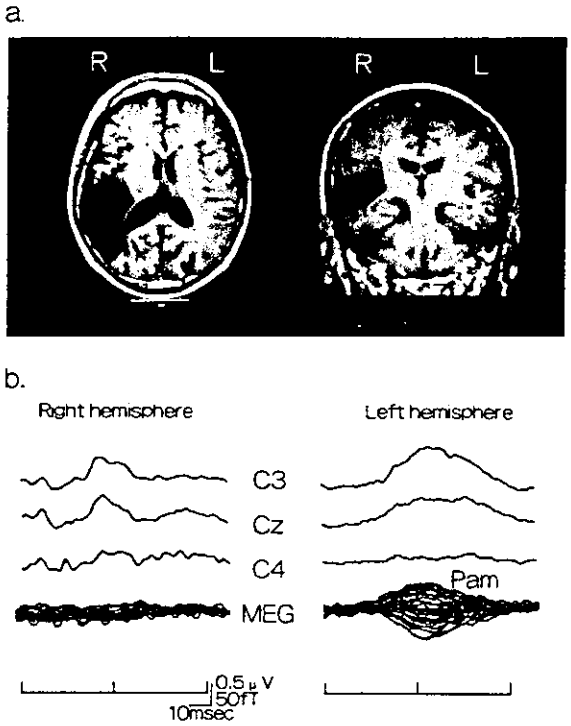

Fig. 4. A typical patient (63-year-old male) with a right auditory cortex lesion in the unilateral temporoparietal infarction. Brain MRI scans. AMLRs and MLAEFs are shown. The MLAEF is absent from the right hemisphere but the Pa is present from both hemispheres.

degeneration or denervation of subcortical structures, such as thalamic projection nuclei, and that this may explain the inconsistency in the presence of the Pa among patients with auditory cortex lesions.

Whereas the Pa reflects activities of several regions, including both auditory cortices, the thalamus and the reticular formation, the Pam, in contrast, almost exclusively reflects the activity of the auditory cortex ipsilateral to the sensor. Therefore, when diagnostic imaging of the auditory cortex is possible, MLAEF analysis with the Pam component as the index is more appropriate than AMLR analysis for functional diagnosis of the auditory cortex.

CONCLUSION

Compared to the Pa component of the AMLR, the Pam of the MLAEF is substantially more sensitive to the activity of the auditory cortex ipsilateral to the magnetic sensor. The primary generator of the Pam in MLAEFs has been demonstrated to be the auditory cortex. However, the Pa of AMLRs is evoked only partly from the auditory cortex because it is evoked even in patients with unilateral auditory cortex lesions.

ACKNOWLEDGEMENTS

We thank Ms M. Nakamura for technical assistance and Ms H Miyazaki for word processing. Roger R. Marsh, PhD of The Children's Hospital of Philadelphia made many helpful comments.

REFERENCES

1. Kaga K, Hink RF, Shinoda Y. Evidence for a primary cortical origin of a middle latency auditory evoked potential in cats. Electroencephalogr Clin Neurophysiol 1980; 50: 254–66.
2. Kraus N, McGee T, Littman T, Nicol T. Reticular formation influences on primary and non-primary auditory pathways as reflected by the middle latency response. Brain Res 1992; 587: 186–94.
3. Kraus N, Özdamar Ö, Hier D, Stein L. Auditory middle latency responses (MLRs) in patients with cortical lesions. Electroencephalogr Clin Neurophysiol 1982; 54: 275–87.
4. Woods DL, Clayworth CC, Knight RT, Simpson GV, Naeser MA. Generators of middle-and long-latency auditory evoked potentials: implications from studies of patients with bitemporal lesions. Electroencephalogr Clin Neurophysiol 1987; 68: 132–48.
5. Ibanez V, Deiber MP, Fisher C. Middle latency auditory evoked potentials in cortical lesions. Criteria of interhemispheric asymmetry. Arch Neurol 1989; 46: 1325–32.
6. Pantev C, Lütkenhöner B, Hoke M, Lehnertz K. Comparison between simultaneously recorded auditory-evoked magnetic fields and potentials elicited by ipsilateral, contralateral and binaural tone burst stimulation. Audiology 1986; 25: 54–61.
7. Pantev C, Hoke M, Lehnertz K, Lütkenhöner B. Neuromagnetic evidence of an amplitopic organization of the human auditory cortex. Electroencephalogr Clin Neurophysiol 1989; 72: 225–31.
8. Pantev C, Bertrand O, Eulitz C, Verkindt C, Hampson S, Schuierer G, et al. Specific tonotopic organization of different areas of the human auditory cortex revealed by simultaneous magnetic and electric recordings. Electroencephalogr Clin Neurophysiol 1995; 94: 26–40.
9. Hall DA, Hart HC, Johnsrude IS. Relationships between human auditory cortical structure and function. Audiol Neurotol 2003; 8: 1–18.
10. Pelizzone M, Hari R, Makela JP, Huttunen J, Ahlfors S, Hamalainen M. Cortical origin of middle-latency auditory evoked responses in man. Neurosci Lett 1987; 82: 303–7.
11. Makela JP, Hamalainen M, Hari R, McEvoy L. Whole-head mapping of middle-latency auditory evoked magnetic fields. Electroencephalogr Clin Neurophysiol 1994; 92: 414–21.
12. Yoshiura T, Ueno S, Iramina K, Masuda K. Effects of stimulation side on human middle latency auditory evoked magnetic fields. Neurosci Lett 1994; 172: 159–62.
13. Kuriki S, Nogai T, Hirata Y. Cortical sources of middle latency responses of auditory evoked magnetic field. Hear Res 1995; 92: 47–51.

Submitted September 1, 2003; accepted September 11, 2003

Address for correspondence:
Kimitaka Kaga
Department of Otolaryngology
Graduate School of Medicine
University of Tokyo
7-3-1 Hongo, Bunkyo-ku
Tokyo 113-8655
Japan
Tel.: +81 3 5800 8665
Fax: +81 3 3814 9486
E-mail: kimikaga-tky@umin.ac.jp

International Journal of Pediatric Otorhinolaryngology (2004) 68, 1115–1119

ELSEVIER

International Journal of Pediatric Otorhinolaryngology

www.elsevier.com/locate/ijporl

CASE REPORT

Hearing evaluation in two sisters with a T8993G point mutation of mitochondrial DNA

Yuki Sakai[a,b,*], Kimitaka Kaga[a,b], Kazuo Kodama[b], Asako Higuchi[c], Junko Miyamoto[c]

[a] *Department of Otolaryngology, School of Medicine, University of Tokyo, 7-3-1, Hongo, Bunkyo-ku, 113-8655 Tokyo, Japan*
[b] *National Center for Children's Rehabilitation, 1-1-10, Komone, Itabashi-ku, 173-0037 Tokyo, Japan*
[c] *Department of Pediatrics, Kiyose Children's Hospital, 1-3-1, Umezono, Kiyose-shi, 204-8567 Tokyo, Japan*

Received 10 September 2003; received in revised form 16 March 2004; accepted 18 March 2004

KEYWORDS
A T8993G point mutation of mitochondrial DNA;
Leigh's syndrome;
Neurogenic muscle weakness, ataxia, and retinitis pigmentosa (NARP);
Sensorineural hearing loss;
Auditory brainstem responses

Summary We report on two sisters with a T8993G point mutation of mitochondrial DNA, and their hearing evaluation. Considering auditory function, hearing in the elder sister remains almost normal. However, in the younger sister, the auditory brainstem response (ABR) threshold has fluctuated remarkably during a 3-year follow-up. The threshold changes of ABR in the younger sister suggest that her hearing problems may well be caused by both cochlear nerves and retrocochlear lesions. Our experience is clinically important because there have been only a few reports on hearing evaluation in patients with a T8993G point mutation of mitochondrial DNA.

1. Introduction

Mitochondrial encephalomyopathies are clinically heterogeneous disorders that can affect skeletal muscle and/or the central nervous system. Hearing loss caused by an inherited mitochondrial mutation has been described and is characterized by a maternal inheritance pattern [1]. In the most frequently encountered syndromes, such as the myoclonic epilepsia with red ragged fibers (MERRF), mitochondrial encephalopathy with lactic acid stroke-like episodes (MELAS), and Kearns–Sayre syndrome (KSS), 30–50% of patients exhibit a hearing loss [2]. Various mitochondrial mutations have been recognized to cause non-syndromal hearing loss. For example, an A1555G substitution in 12S ribosomal RNA in the mitochondrial genome together with exposure to an otherwise non-toxic aminoglicoside antibiotic or an additional genetic factor can lead to hearing impairment [3]. Similarly, an A3243G point mutation in the $tRNA^{Leu}$ gene has been associated with diabetes mellitus and sensorineural hearing loss [4]. Regarding mutations affecting the $tRNA^{(Ser)(UCN)}$ gene in mitochondria, four different mutations have been identified, all of which

*Corresponding author. Present address: ATORU MASAGO 701, 1-35-27 Hongo, Bunkyo-ku, 113-0033 Tokyo, Japan.
Tel.: +81-3-5800-8665; fax: +81-3-3814-9486.
E-mail address: xxxsakai@livedoor.com (Y. Sakai).

0165-5876/$ – see front matter © 2004 Elsevier Ireland Ltd. All rights reserved.
doi:10.1016/j.ijporl.2004.03.015

causes sensorineural hearing loss [2]. The A7445G point mutation in the $tRNA^{(Ser)(UCN)}$ gene causes not only hearing loss but palmoplantar keratoderma as well [5]. Hearing loss, ataxia and myoclonus were present in a large kindred from Sicily with a heteroplasmic C7472 nucleotide insertion in the same gene [6]. A mentally retarded 26-year-old woman with a T7512C mutation in this gene who suffered from myoclonic seizures, muscle atrophy weakness, and hearing disturbances lasting for a few seconds has also been documented [7]. In addition to these mutations, the T7510C mutation was described in a small family of 10 individuals with non-syndromal sensorineural hearing impairment [8]. In patients with these mutations, the age of hearing loss onset ranges from congenital to adulthood, and the severity ranges from mild to severe [2]. To our knowledge, descriptions of hearing loss in patients with a T8993G point mutation of mitochondrial DNA are only a few. A T8993G point mutation was first reported by Holt et al. [9] to cause a variable combination of developmental delay, retinitis pigmentosa, dementia, seizure, ataxia, and proximal neurogenic muscle weakness. They examined blood and muscle from patients to determine whether a correlation existed between clinical severity and the amount of mutant mitochondrial DNA. Following this report, Tatuch et al. [10] described how a heteroplasmic mitochondrial DNA mutation at T8993G could cause Leigh's syndrome when the percentage of abnormal mitochondrial DNA was high. This association was confirmed by other workers [11,12]. In these reports, hearing loss in the patients was not described. We investigated hearing in two sisters who have Leigh's syndrome with a T8993G point mutation of mitochondrial DNA using auditory brainstem response (ABR) and we found ABR abnormalities in the younger sister.

2. Case report

Two sisters (currently 11- and 4-year-old) experienced repeated epileptic seizures several months after birth. They were examined in Kiyose Children's Hospital. Brain CT scanning showed bilateral low density areas in the basal ganglia and the posterior limb of the internal capsule. They were suspected of having Leigh's syndrome associated with a mitochondrial disease. In the clinical findings, lactate and pyruvate levels were high in the spinal fluid in the elder sister, and those acids were high in both the serum and spinal fluid in the younger sister. They had neurogenic muscle weakness, ataxia, and retinitis pigmentosa (NARP) as well as epileptic seizures, and were also mentally

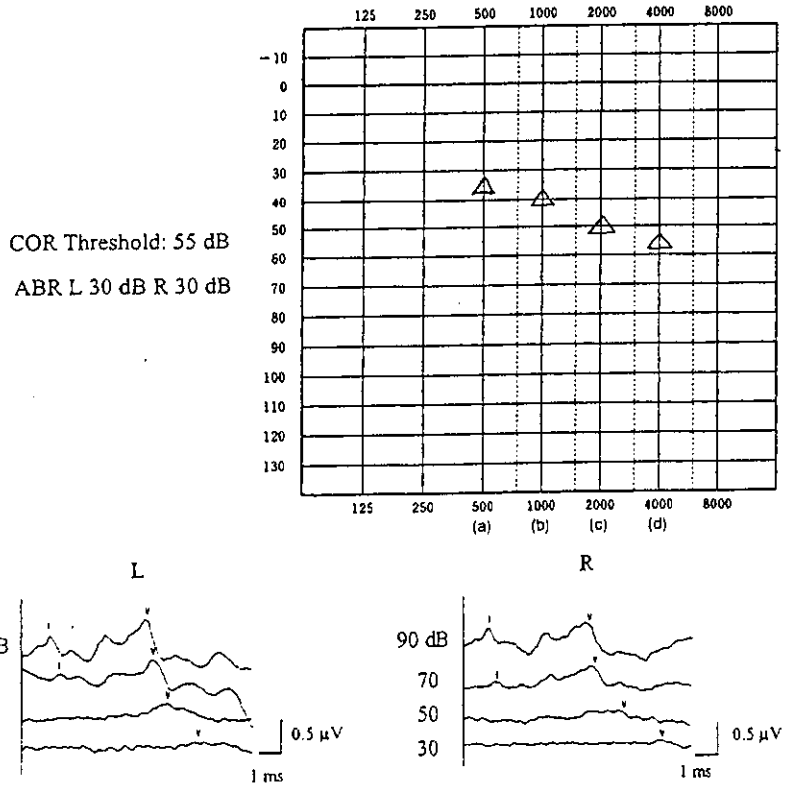

Fig. 1 COR and ABR at 8 years of age in the elder sister (L: left ear, R: right ear).

retarded. No abnormalities were found in glucose tolerance. They were diagnosed as having a T8993G point mutation of mitochondrial DNA based on the results of genetic evaluation. Their mother had the same mutation, but was asymptomatic. She had no hearing loss. Because these sisters had poor response to sound, they were referred to our hospital for hearing evaluation when the elder sister was 8 years old and the younger sister was 8 months.

2.1. Elder sister

The otoscopic findings revealed no abnormalities. Fig. 1 shows the results of conditioned response audiometry (COR) and ABR in the elder sister when she was 8 years old. The COR threshold was slightly elevated (55 dB). In the first ABR measurement, the threshold was 30 dB in both ears. Peak latency of wave I and wave V, and peak interval of wave I–V at 90 dB were not delayed (Table 1). The COR threshold has not changed since that time.

2.2. Younger sister

Fig. 2 shows the measurement of ABR in the younger sister at 8 months, 1 year, 1.5 years, and 3 years of age. The otoscopic findings showed no abnormalities. At 8 months, the threshold was 20 dB in both ears. However, the threshold was elevated to 90 dB in the left ear and 70 dB in the right at 1 year of age. The threshold had improved in the younger sister at 1 year and 5 months of age to 30 dB in both ears. However, it deteriorated to 70 dB in the left ear and 90 dB when she was 3 years old, with low

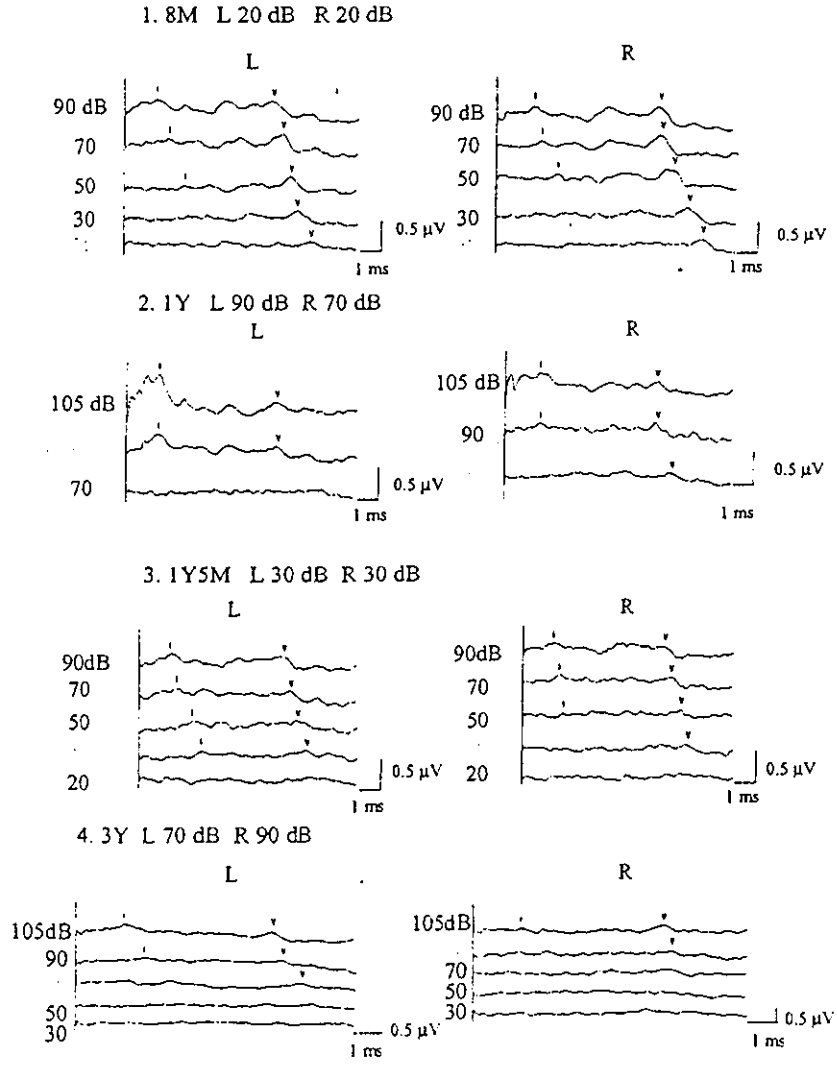

Fig. 2 The measurement of ABR in the younger sister at 8 months, 1 year, 1.5 years and 3 years of age (M: months of age, Y: years of age, L: left ear, R: right ear).

Table 1 Peak latency of wave I and wave V, and peak interval of wave I–V at 90 dB in ABR

	Age	Wave I peak latency (ms)	Wave V peak latency (ms)	Wave I–V peak interval (ms)
Elder sister	8 Y	R 1.35, L 1.25 (1.39 ± 0.07)	R 5.49, L 5.37 (5.42 ± 0.25)	R 4.14, L 4.12 (4.03 ± 0.31)
Younger sister	8 M	R 1.46, L 1.58 (1.42 ± 0.06)	R 6.59, L 6.38 (5.94 ± 0.20)	R 5.13, L 4.80 (4.52 ± 0.13)
	1 Y	R 1.43, L 1.50 (1.41 ± 0.09)	R 6.51, L 6.42 (5.92 ± 0.23)	R 5.08, L 4.92 (4.51 ± 0.19)
	1.5 Y	R 1.39, L 1.48 (1.41 ± 0.09)	R 6.87, L 6.61 (5.92 ± 0.23)	R 5.48, L 5.13 (4.51 ± 0.19)
	3 Y	R (−), L 1.47 (1.45 ± 0.04)	R 6.51, L 6.25 (5.66 ± 0.08)	R (−), L 4.78 (4.21 ± 0.11)

Mean and S.D. of the control data are shown under each result, M: months of age, Y: years of age).

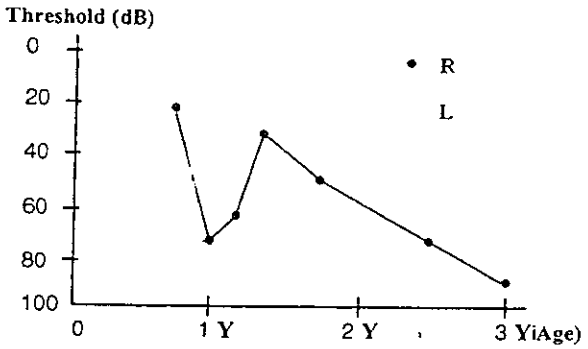

Fig. 3 A line graph of the threshold changes in ABR from 8 months to 3 years of age in the younger sister. The vertical axis is the threshold and the horizontal axis is her age (Y: years of age).

amplitude. Her COR was uncertain. In each recording of the ABR, peak latency of wave I and wave V, and peak interval of wave I–V at 90 dB were delayed compared with those from our age-matched control data (Table 1). A distortion products otoacousitic emissions (DPOAE) study revealed normal DPOAE.

By the age of 3 years, we had recorded ABR seven times in the younger sister. Fig. 3 shows a line graph of the threshold changes in her ABR. The threshold was normal at 8 months, but it had deteriorated markedly by the time she reached 1 year of age, and afterward it improved rapidly, however, subsequently it gradually worsened.

3. Discussion

Hearing in the elder sister is almost normal based on the results of the COR and ABR measurement. In the younger sister, she had no abnormalities at delivery and a few months after birth. Considering the results of her DPOAE tests, her bilateral inner ears are almost normal. However, the amplitude of the ABR at 3 year of age was low. These findings of DPOAE and ABR indicate that the responsible lesion causing hearing loss in the younger sister might involve the cochlear nerves. Moreover, the peak latency of wave I and wave V and the peak interval of wave I–V at 90 dB are markedly delayed. These findings demonstrate that retrocochlear problems exist in her hearing loss. Kaga et al. [13] reported auditory brainstem responses in Leigh's syndrome. They studied the lesions in patients with Leigh's syndrome using brain CT and ABRs. Abnormalities of ABRs were detected in the early stages of the disease in all patients but ABR configurations differed in the lesion. In some patients with the cortical form of Leigh's syndrome, the configuration became nearly flat with the passage of time. That was similar to our observations. Yoshinaga et al. [14] noted an abnormality in the ABR from the early stages in a child with a T8993G point mutation of mitochondrial DNA. III–V interpeak latency of the child was prolonged, and wave V amplitude was low at the age of 7 months. After that, the auditory response deteriorated, and loss of all components was demonstrated at the age of 3 years 5 months. This result was the same as ours. It was thought that the retrocochlear problems in our younger patient must be related to Leigh's syndrome. In regards to heteroplasmy, Yoshinaga et al. [14] described the clinical course of patients with a T8993G point mutation will change according to proportionality of mutant and wild type mitochondrial DNA and to what organs are affected most, while several reports emphasized the degree of hearing loss was not clearly correlated with the amount of the mutant mitochondrial DNA, indicating that other, yet unidentified factors are responsible in other mitochondrial disorders [2,15,16]. Therefore, the definitive reason for the fluctuating hearing loss in our case remains unknown. In terms of auditory behavior, the elder sister can locate sound sources easily and can engage in limited communication with others through gestures. The younger sister responded to sounds better when her ABR threshold improved. We thought that it would be difficult to fit the younger sister with a hearing aid because of the fluctuation in the threshold and her mental retardation.

References

[1] N. Fischel-Ghodsian, Mitochondrial mutations and hearing loss-paradigm for mitochondrial genetics, Am. J. Hum. Genet. 62 (1998) 15–19.

[2] W.R.J. Cremers Cor, R.J.H. Smith (Eds.), Genetic Hearing Impairment Adv. Otolaryngol., vol. 61, Basel, Kerger, 2002, pp. 172–183.

[3] T.R. Prezant, J.V. Agapian, M.C. Bohlman, Mitochondrial ribosomal RNA mutation associated with both antibiotic-induced on non-syndromic deafness, Nature Genet. 4 (1993) 289–294.

[4] S. Manouvrier, A. Rotig, G. Hannebique, Point mutation of the mitochondrial $tRNA^{Leu}$gene (A3243G) in maternally inherited hypertrophic cardiomyopathy, diabetes mellitus, renal failure, and sensorineural deafness, J. Med. Genet. 32 (1995) 654–656.

[5] F.M. Reid, G.A. Vernham, H.T. Jacobs, Complete mt DNA sequence of a patients in a maternal pedigree with sensorineural deafness, Hum. Mol. Genet. 3 (1994) 1435–1436.

[6] V. Tiranti, P. Chariot, Carella, Hum. Mol. Genet 4 (1995) 1421–1427.

[7] M. Nakamura, S. Nakano, Y.I. Gato, A novel point mutation in the mitochondrial $tRNA^{(Ser)(UCN)}$gene detected in a family with MERRF/MELAS overlap syndrome, Biochem. Biophys. Res. Commun. 214 (1995) 86–93.

[8] T. Hutchin, M.J. Parker, I.D. Young, A novel mutation in the mitochondrial $tRNA^{(Ser)(UCN)}$gene in a family with non-syndromal sensorineural hearing impairment, J. Med. Genet. 37 (2000) 692–694.

[9] I.J. Holt, A.E. Harding, R.K.H. Petty, A new mitochondrial disease associated with mitochondrial DNA heteroplasmy, Am. J. Hum. Genet. 46 (1990) 428–433.

[10] Y. Tatuch, J. Christodoulou, A. Feigenbaum, Heteroplasmic mtDNA mutation (T → G) at 8993 can cause Leigh disease when the percentage of abnormal mtDNA is high, Am. J. Hum. Genet. 50 (1992) 852–858.

[11] F.M. Santorelli, S. Shanske, A. Macaya, The mutation at nt 8993 of mitochondrial DNA is a common cause of Leigh's syndrome, Ann. Neurol. 34 (6) (1993) 827–834.

[12] J.M. Soffner, P.M. Fernhoff, N.S. Krawiecki, Subacute necrotizing encephalopathy: oxidative phosphorylation defects and the ATPase 6 point mutation, Neurol. 42 (1992) 2168–2174.

[13] M. Kaga, H. Naitoh, K. Nihei, Auditory brainstem response in Leigh's syndrome, Acta Paediatr. Jpn. 29 (1987) 254–260.

[14] H. Yoshinaga, T. Ogino, S. Ohtahara, A T-to-G mutation at nucleotide pair 8993 in mitochondrial DNA in a patient with Leigh's syndrome, J. Child Neurol. 8 (2) (1993) 129–133.

[15] F. Reid, A. Rovio, I.J. Holt, Molecular phenotype of a human lynphoblastoid cell line homoplasmic for the np7445 deafness-associated mitochondrial mutation, Hum. Mol. Genet. 6 (1997) 443–449.

[16] R.J.H. Ensink, H.A.M. Marres, C.W.R.J. Cremers, Early-onset maternal inherited hearing loss with late-onset neurological symptoms present in a three-generation Dutch family, in: Proceedings of the Second Workshop European Working Group on Genetics of Hearing Impairment, Milan, October 1996.

Acta Otolaryngol 2004; Suppl 553: 23–27

Taylor&Francis
healthsciences

Actions of Subtype-specific Purinergic Ligands on Rat Spiral Ganglion Neurons

KEN ITO[1], SHINICHI IWASAKI[1], KENJI KONDO[1], DIDIER DULON[2] and KIMITAKA KAGA[1]

From the [1]Department of Otolaryngology, Faculty of Medicine, University of Tokyo, Tokyo, Japan and [2]Laboratoire de Biologie Cellulaire et Moléculaire de l'Audition, INSERM EMI 99-27, Université de Bordeaux 2, Hôpital Pellegrin Bat PQR, Bordeaux, France

Ito K, Iwasaki S, Kondo K, Dulon D, Kaga K. *Actions of subtype-specific purinergic ligands on rat spiral ganglion neurons.* Acta Otolaryngol 2004; Suppl 553: 23–27.

In a previous study we showed that, in rat spiral ganglion neurons (SGNs), the adenosine 5′-triphosphate (ATP)-evoked currents were a combination of the activation of ionotropic receptors (the first fast current) and the activation of metabotropic receptors which secondarily opened non-selective cation channels. These two conductances imply the involvement of different receptor subtypes. In the present study, we tested three subtype-specific purinergic ligands: α,β-methylene ATP (α,β-meATP) for P2X receptors, uridine 5′-triphosphate (UTP) for P2Y receptors and 2′-3′-O-(4-benzoylbenzoyl) ATP (Bz-ATP) for P2Z ($P2X_7$) receptors. Application of 100 μM α,β-meATP did not trigger any significant change in membrane conductance, while the SGNs were responsive to ATP. Pressure application of UTP (100 μM, 1 s) evoked an inward current averaging 344±169 pA at a holding potential of −50 mV. The conductance developed after a latency averaging 1.5±0.6 s, took 4–6 s to peak and reversed slowly within 15–30 s. The current–voltage curve reversed near 0 mV, suggesting a non-selective cation conductance, like the second component of the ATP conductance. Bz-ATP evoked an inward current which developed without latency, was sustained during ligand application and was rapidly inactivated at the end of application: the same characteristics as the first component of the ATP-evoked current. The Bz-ATP conductance reversed around −10 mV, indicating also a non-selective cation conductance. These results suggest that, in SGNs, ATP acts via two different receptor subtypes, ionotropic P2Z receptors and metabotropic P2Y receptors, and that these two receptor subtypes can assume different physiological roles. *Key words: P2X, P2Y, P2Z, purinergic receptor, spiral ganglion neuron.*

INTRODUCTION

While glutamate is recognized as the principal neurotransmitter at the inner hair cell–spiral ganglion neuron (SGN) synapse, other neurochemicals, including adenosine 5′-triphosphate (ATP), have been proposed to act as neuromodulators at the efferent synapse on the SGNs (1). The existence of purinergic receptors on SGNs has been shown by autoradiography (2), in situ hybridization (3) and immunolocalization (4) techniques. These receptors were found to be physiologically functional as the result of in vivo (5) and in vitro (4, 6) studies. We recently reported (7) a depolarizing cation non-selective conductance evoked by ATP in rat SGNs. Figure 1 summarizes the typical characteristics of this conductance. Brief application of ATP evoked a reversible inward current (Fig. 1a). The current evoked by ATP displayed two components: a first fast component without latency and a second slow component with a latency of ≈1 s. The second component was larger in amplitude, took 3–4 s to peak and reversed slowly within 15–30 s. The two components of the purinergic response could be easily separated and identified using a very brief application of ATP. Analysis of the current–voltage (I–V) relationship of this second component indicated a large increase in membrane conductance during application of ATP (Fig. 1b). ATP-evoked currents displayed an inward rectification at negative potentials and were reversed near 0 mV, indicating the activation of a non-selective cation conductance. These results suggested that the ATP-evoked currents were a combination of the activation of ionotropic receptors (the first fast current) and the activation of metabotropic receptors which secondarily opened non-selective cation channels. These two conductances imply the involvement of different receptor subtypes having different physiological roles. In the present study, we tested three subtype-specific purinergic ligands: α,β-methylene ATP (α,β-meATP) for P2X receptors, uridine 5′-triphosphate (UTP) for P2Y receptors and 2′-3′-O-(4-benzoylbenzoyl) ATP (Bz-ATP) for P2Z ($P2X_7$) receptors (8).

MATERIAL AND METHODS

Preparation of SGNs

Detailed procedures for freshly isolating SGNs have been published elsewhere (9). Briefly, rats (3–7 days old) were deeply anesthetized with an i.p. injection of 0.1–0.2 ml of a solution consisting of 1 volume of 50 mg/ml ketamine and 1 volume of 2% xylazine, and then decapitated. Cochleae were extracted from the temporal bone and bathed in Dulbecco's phosphate-buffered saline containing (mM): NaCl, 136.9; Na_2HPO_4, 6.5; KCl, 2.7; KH_2PO_4, 1.5; $CaCl_2$, 0.9; and $MgCl_2$, 0.5, with the pH adjusted to 7.3. The shell was opened and the stria vascularis and the organ of Corti were removed. Spiral ganglions were extracted from the spiral lamina of the two basal turns. The SGNs were isolated by mechanical dissociation following enzymatic treatment with trypsin (type III; 100 μg/ml, 37°C, 30 min) on glass coverslips (diameter 30 mm, thickness 0.13–0.17 mm) sealed in the middle of

 ISSN 0365-5237

DOI 10.1080/03655230410017616

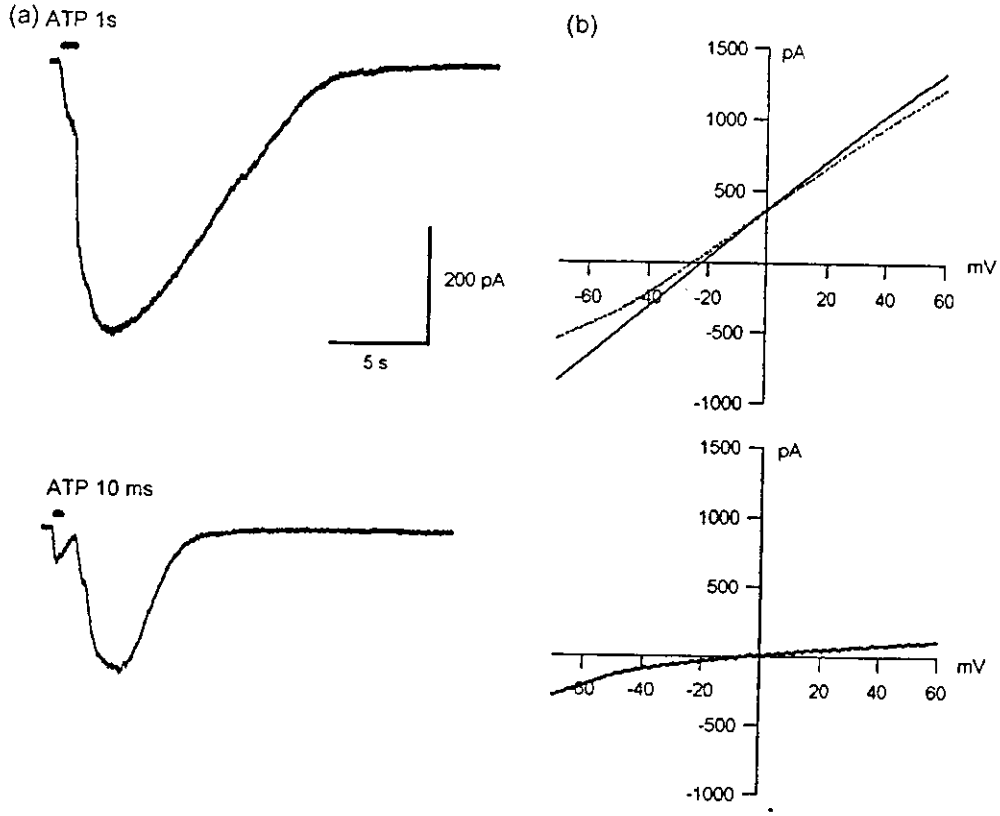

Fig. 1. (a) Top trace: a brief application (1 s) of ATP (100 μM) evoked a reversible inward current under the voltage-clamp condition at −50 mV. Bottom trace: the two purinergic components could be isolated in the time domain by using a very short (10 ms) application of ATP (100 μM). The same SGN was held at −50 mV. (b) Example of a typical I–V relationship obtained using the ramp protocol in an SGN stimulated with 100 μM ATP. Upper: solid and dotted traces represent the currents during and without activation of the second component of the purinergic (ATP) conductance, respectively. Lower: the purinergic current obtained by subtraction.

perforated Petri dishes (35 mm diameter; Nunc). Before starting the experiments, SGNs were left to rest for at least 2 h at room temperature. Identification of SGNs under a microscope was facilitated by their shape and grouping and by the remnants of dendrites or axons (9). Our results were obtained essentially from type I SGNs, which represented >95% of the cells in our preparation. Type I SGNs from newborn rats could be distinguished from the rare type II SGNs by their larger size and the presence of a soft, thin myelin shield.

Electrophysiological recordings

Recordings on SGNs were performed with the conventional whole-cell patch clamp configuration, using an Axopatch-1D amplifier (Axon Instruments, Foster City, CA). Electrodes were pulled from borosilicate glass capillaries (GC150TF-10; Clark Electromedical, UK). The internal solution consisted of (mM): KCl, 158; KOH, 3.5; $MgCl_2$, 2.0; ethylene glycol tetraacetic acid, 1.1; and 4-(2-hydroxyethyl)-1-piperazinethansulfonic acid, 5.0, with the pH adjusted to 7.2 and the osmolality adjusted to 300 mOsm. Axotape and pCLAMP software (Axon Instruments) and IGOR Pro software (Wavemetrics Inc., Lake Oswego, OR) were used for data collection and analysis. Junction potentials were set to zero immediately before gigaseal formation. Electrode resistance ranged from 3 to 6 MΩ. The electrode capacitance and series resistance were not corrected at the time of experimentation. I–V relationships were obtained from voltage ramps (−80 mV to +70 mV, 900 ms) and corrected for series resistance-induced voltage errors. The ramp protocol started from a holding potential of −50 mV, jumped to −80 mV for 20 ms and then swept linearly to +70 mV over a 900-ms period. In order to measure the I–V relationship during agonist stimulation, we started the ramp protocol at the peak current.

Drug application

Test solutions were applied to SGNs using a Picospritzer puffer system (Picospritzer II; General Valve, Fairfield, NJ) as previously described (10). Puff pipettes were pulled similarly to the recording patch clamp pipettes. The tips of the pipettes were placed ≈20–40 μm from the SGNs. The delay for drugs to

reach the cell ranged from 20 to 50 ms (10). When repetitive applications of drugs were made to the same SGN, we waited for at least 2 min between applications in order to reduce desensitization.

All experiments were performed at room temperature (20–22°C). All reagents were purchased from Sigma Chemical Company. The data are expressed as mean ± SD unless specifically noted otherwise.

RESULTS

Responses to the P2X ligand

Application of 100 μM α,β-meATP did not trigger any significant change in membrane conductance, while the SGNs were responsive to ATP ($n = 5$; Fig. 2).

Responses to the P2Y ligand

Under the whole-cell voltage clamp condition, pressure application of UTP (100 μM, 1 s) evoked an inward current in 71% of tested SGNs ($n = 17$; Fig. 3a), averaging 344 ± 169 pA at a holding potential (Vh) of −50 mV. The conductance developed after a latency averaging 1.5 ± 0.6 s, took 4–6 s to peak and reversed slowly within 15–30 s. Analysis of the I–V relationship of the UTP response, tested with a voltage-ramp protocol, indicated a large increase in membrane conductance (Fig. 3b). The I–V curve showed inward rectification at negative membrane potentials and was reversed at 3.3 ± 8.6 mV ($n = 4$). These results demonstrated that UTP activated a non-selective cation conductance, like the second component of the ATP conductance. The long delay between ligand application and activation of conductance confirms the involvement of metabotropic processes evoked by P2Y receptors.

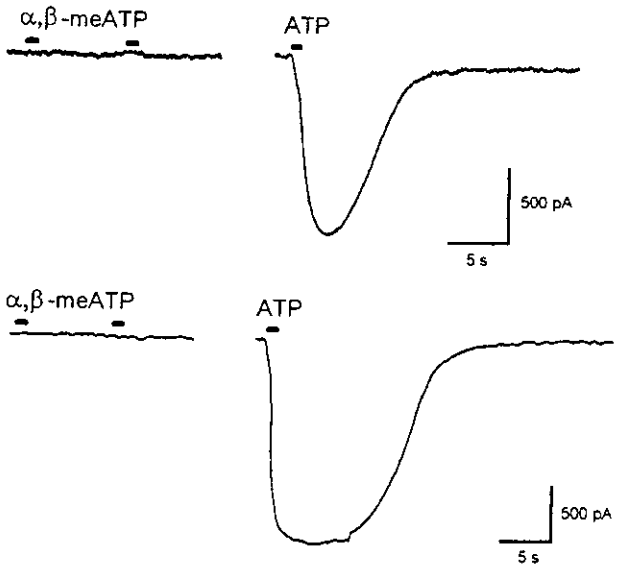

Fig. 2. Application of α,β-meATP (100 μM, 1 s) did not evoke a current while the SGNs were responsive to ATP (Vh = −50 mV). Two examples are shown.

Responses to the P2Z ligand

Under the whole-cell voltage clamp condition, pressure application of Bz-ATP (100 μM, 1 s) evoked an inward current in 69% of tested SGNs ($n = 16$; Fig. 4a). The Bz-ATP current developed without latency, was sustained during Bz-ATP application and was rapidly inactivated at the end of the ligand application: the same characteristics as the first component of the ATP-evoked current [see Fig. 5a of our previous paper (7)]. The I–V relationship of the Bz-ATP response, measured during prolonged ligand application, also indicated an increase in membrane conductance (Fig. 4b). The Bz-ATP conductance reversed at −11.7 ± 13.0 mV ($n = 4$), indicating also a non-selective cation conductance, but with a smaller permeability than that of the ATP-evoked second component and the UTP conductance.

DISCUSSION

In summary, the present results showed that Bz-ATP, a P2Z ligand, and UTP, a P2Y ligand, evoked current responses very similar to the first and second components of the ATP response, respectively. No measurable responses occurred with α,β-meATP, a P2X ligand. In SGNs, P2Y receptors are supposed to mobilize intracellular calcium (6) and to open, via metabotropic processes, the large cation non-selective channels which have been shown to be shared by various ligands (7, 11). P2Z receptors are known to increase cell permeability by opening large cation non-selective channels (8), which is consistent with our present results. Although P2Z receptors have been demonstrated in the central nervous system (12), this is the first report of functional P2Z receptors in SGNs. Regarding P2X receptors in rat SGNs, there remains scope for their possible involvement, as α,β-meATP has been shown to be inactive with certain subtypes of P2X receptors, e.g. $P2X_2$, $P2X_5$ and $P2X_6$, in certain cell types (8). However, there is no more perfectly subtype-specific ligand. For example, 2-methylthio ATP is a more potent ligand for P2X receptors but also interacts with P2Y receptors. Involvement of different types of receptors can suggest different physiological roles. P2Z ($P2X_7$) receptors were initially considered to cause cell lysis by increasing cell permeability but were subsequently postulated to mediate fast synaptic transmission or modulation (12). In contrast, P2Y receptors may regulate neuronal excitability more slowly by changing the resting potential. Moreover, P2Y receptors may affect neuronal survival by increasing the intracellular calcium

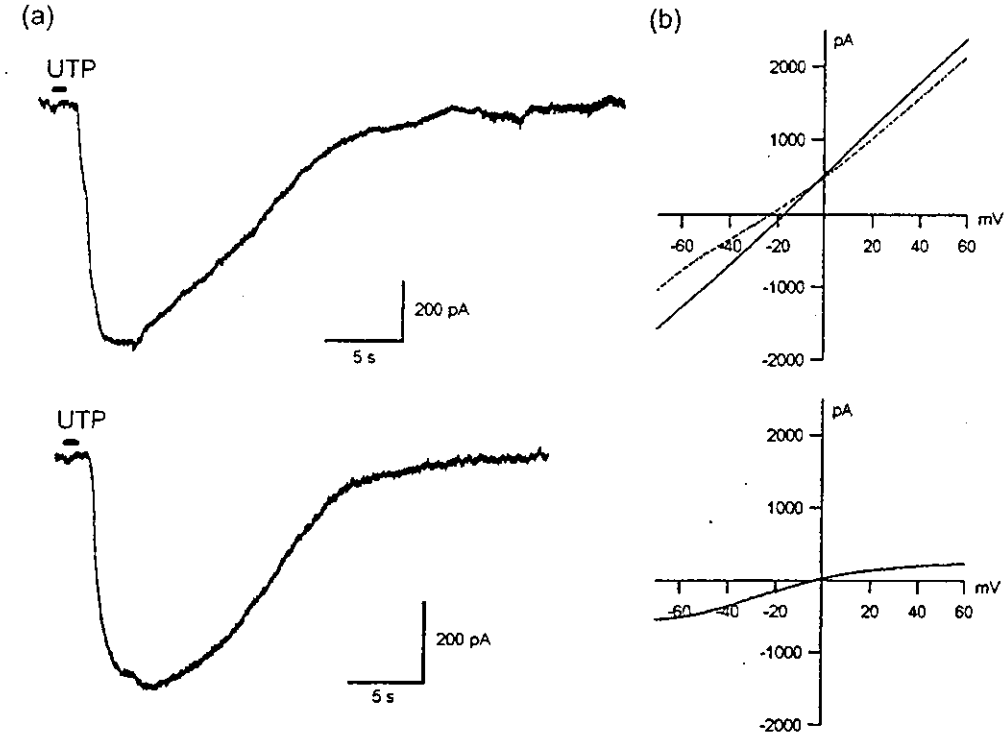

Fig. 3. (a) Brief application (1 s) of UTP (100 μM) evoked a reversible inward current under the voltage-clamp condition at −50 mV. The conductance was evoked with a latency of ≈1.5 s, i.e. it developed after application of the ligand ceased. Two examples are shown. (b) Example of a typical I–V relationship obtained using the ramp protocol in an SGN stimulated with 100 μM UTP. Upper: solid and dotted traces represent the currents during and without activation of the UTP conductance, respectively. Lower: the UTP current obtained by subtraction.

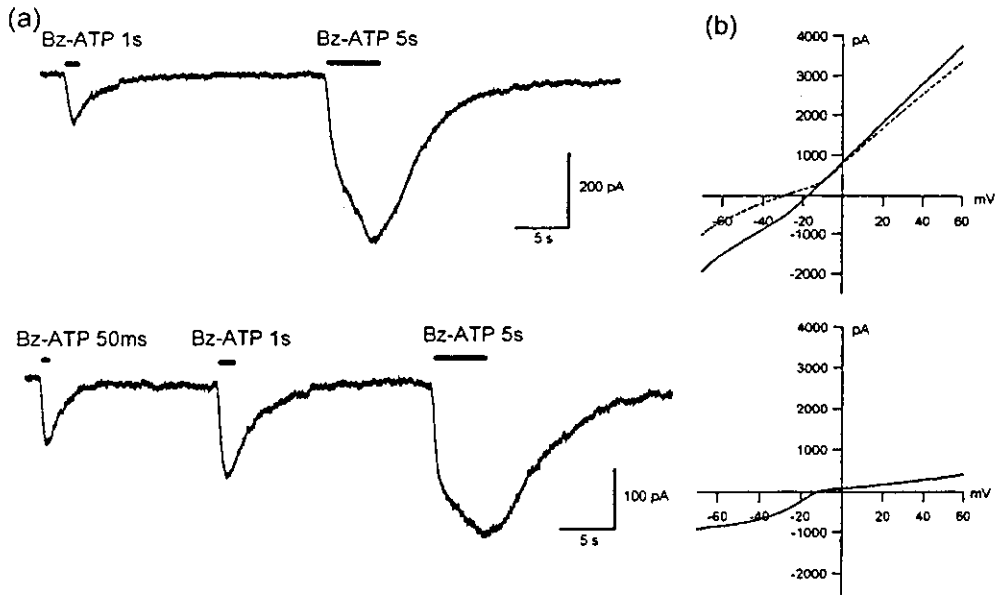

Fig. 4. (a) Examples of Bz-ATP-evoked conductance. The current developed without latency, was sustained during ligand application (100 μM Bz-ATP) and was inactivated rapidly after application had ceased. The SGN was held at −50 mV. (b) Example of a typical I–V relationship obtained using the ramp protocol in an SGN stimulated with 100 μM Bz-ATP. Upper: solid and dotted traces represent the currents during and without activation of the Bz-ATP conductance, respectively. Lower: the Bz-ATP current obtained by subtraction.

concentration (13). More intensive in vivo studies are required in order to determine precisely the physiological effects of these purinergic receptors on SGNs.

ACKNOWLEDGEMENT

Part of this work was supported by the Canon Foundation Europe (Leiden, The Netherlands).

REFERENCES

1. Eybalin M. Neurotransmitters and neuromodulators of the mammalian cochlea. Physiol Rev 1993; 73: 309–73.
2. Mockett BG, Bo X, Housley GD, Thorne PR, Burnstock G. Autoradiographic labelling of P2 purinoceptors in the guinea-pig cochlea. Hear Res 1995; 84: 177–93.
3. Housley GD, Luo L, Ryan AF. Localization of mRNA encoding the P2X2 receptor subunit of the adenosine 5′-triphosphate-gated ion channel in the adult and developing rat inner ear by in situ hybridization. J Comp Neurol 1998; 393: 403–14.
4. Salih SG, Housley GD, Raybould NP, Thorne PR. ATP-gated ion channel expression in primary auditory neurones. Neuroreport 1999; 10: 2579–86.
5. Chen C, Skelett RA, Fallon M, Bobbin RP. Additional pharmacological evidence that endogenous ATP modulates cochlear mechanics. Hear Res 1998; 118: 47–61.
6. Cho H, Harada N, Yamashita T. Extracellular ATP-induced $Ca2^+$ mobilization of type I spiral ganglion cells from the guinea pig cochlea. Acta Otolaryngol (Stockh) 1997; 117: 545–52.
7. Ito K, Dulon D. Nonselective cation conductance activated by muscarinic and purinergic receptors in rat spiral ganglion neurons. Am J Physiol Cell Physiol 2002; 282: C1121–35.
8. Ralevic V, Burnstock G. Receptors for purines and pyrimidines. Pharmacol Rev 1998; 50: 413–92.
9. Rome C, Luo D, Dulon D. Muscarinic receptor-mediated calcium signaling in spiral ganglion neurons of the mammalian cochlea. Brain Res 1999; 846: 196–203.
10. Blanchet C, Erόstegui C, Sugasawa M, Dulon D. Acetylcholine-induced potassium current of guinea-pig outer hair cells: its dependence on a calcium influx through nicotinic-like receptors. J Neurosci 1996; 16: 2574–84.
11. Ito K, Rome C, Bouleau Y, Dulon D. Substance P mobilizes intracellular calcium and activates a nonselective cation conductance in rat spiral ganglion neurons. Eur J Neurosci 2002; 16: 2095–102.
12. Surprenant A, Rassendren F, Kawashima E, North RA, Buell G. The cytolytic P2Z receptor for extracellular ATP identified as a P2X receptor (P2X7). Science 1996; 272: 735–8.
13. Hegarty JL, Kay AR, Green SH. Trophic support of cultured spiral ganglion neurons by depolarization exceeds and is additive with that by neurotrophins or cAMP and requires elevation of [Ca2+]i within a set range. J Neurosci 1997; 17: 1959–70.

Address for correspondence:
Ken Ito, MD
Department of Otolaryngology
Faculty of Medicine
University of Tokyo
7-3-1 Hongo, Bunkyo-ku
Tokyo 113-8655
Japan
Tel.: +81 3 5800 8665
Fax: +81 3 3814 9486
E-mail: itoken-tky@umin.ac.jp

Cortical mapping of auditory-evoked offset responses in rats

Hirokazu Takahashi,[CA] Masayuki Nakao and Kimitaka Kaga[1]

Department of Engineering Synthesis, Graduate School of Engineering, The University of Tokyo, Tokyo, 113-8656, Japan; [1]Department of Otolaryngology, and Head and Neck Surgery, Graduate School of Medicine, The University of Tokyo, 7-3-1 Hongo, Bunkyo-ku, Tokyo, 113-8655, Japan

[CA]Corresponding Author: hiro@hnl.t.u-tokyo.ac.jp

Received 6 April 2004; accepted 17 May 2004

DOI: 10.1097/01.wnr.0000134848.63755.5c

We characterized the auditory-evoked offset responses of the rat auditory cortex by multiple-site surface microelectrode recording. Tone bursts served as test stimuli. Offset responses did not appear tonotopically, but at the fringe of tonotopic onset distributions. Offset amplitude was significantly sensitive to sound intensity, fall time at tone termination, and duration. These results suggest that offset responses are associated with inhibitory responses surrounding excitatory onset responses, and offset responses become large when inhibition becomes strong and long or terminates synchronously. Thus, the rebound after the inhibition in the presence of a stimulus is likely to be a major cause of offset responses in the auditory cortex. *NeuroReport* 15:1565–1569 © 2004 Lippincott Williams & Wilkins.

Key words: Auditory cortex; Auditory evoked potential; Duration tuning; Functional organization; Off neuron; Offset response; Rat; Surface microelectrode array

INTRODUCTION

Auditory-evoked offset responses that appear after the cessation of auditory stimuli under particular conditions have been described in auditory brain stem response (ABR) studies [1,2] and in MEG studies of the auditory cortex [3,4]. Many unit studies also found that 10–30% of auditory neurons selectively respond after the termination of stimuli, from the auditory nerve [5] through the brain stem pathway [6–14] to cortex [5,15–17], and these neurons are called off neurons.

Many off neurons in the inferior colliculus or more central nuclei are duration-sensitive, suggesting that they are involved in the temporal integration of auditory information and encoding of the amplitude change of the sound signal envelope [5–16]. Interestingly, these neurons are sometimes tuned to biologically important information and thereby considered to be context-dependent. For example, duration-tuned neurons in the frog auditory midbrain are commonly tuned in the range of 100 ms or less, corresponding to the duration of the frog's mating calls [6]. Many off neurons in the bat are tuned to the best frequency between 58 and 62 kHz and duration between 2 and 10 ms, which are similar to the ranges of the frequency and duration of their echolocation calls [5,7,9,16].

Previous studies, however, have not satisfactorily characterized the offset response properties particularly at the auditory cortex level. The small number of off neurons, as compared with on neurons, may hamper the detailed characterization of offset responses, particularly in terms of the place code, resulting in fragmentary information. To bridge previous fragmentary investigations, we densely map tone-burst evoked potentials over the auditory cortex and examine the overall characteristics of offset responses.

MATERIALS AND METHODS

Experimental procedure: We used a surface microelectrode array to epipially map auditory evoked potentials (AEP) in the auditory cortex of rats [18]. The array had 10 × 7 recording points in a 3.5 × 3 mm area that covered the majority of the auditory cortex including the primary, anterior, and ventral auditory field (AI, AAF and VAF). Sixty-four out of 70 recording points were selected for the recording.

Twelve adult Wister rats, weighing 200–350 g, were used. Each rat was anesthetized with ketamine (50 mg/kg, i.m.) and xylazine (10 mg/kg, i.m.), and fixed to a stereotaxic holder. The temporal bone and dura mater were partly removed to expose the auditory cortex. We inserted a reference electrode at the vertex and a ground electrode 7 mm anterior to the vertex, and mounted the surface microelectrode array on the auditory cortex.

Cortical evoked potentials from 64 recording sites were amplified simultaneously with a gain of 1000, filtered with a passband of 0.5–1500 Hz, −12 dB/octave, and digitized at a sampling rate of 200 μs. A speaker placed 20 cm from an ear,

Table 1. Tone bursts used in the experiments: I, intensity; F, frequency; RF, rise-fall time; and D, duration.

I (dBSPL)	F (kHz)	RF (ms)	D (ms)
40, 60, 80	5	1, 5, 10, 20	300
60	5	5	200, 300, 500
80	5, 20, 40	5	300

contralateral to the exposed cortex, delivered acoustic stimuli with a repetition rate of 0.5–0.9/s. The stimuli delivered were monitored by a microphone placed near the auricle and presented in dBSPL (sound pressure level in dB re 20 μPa). Tone bursts were used as test stimuli, and frequency, intensity, rise and fall time, and duration served as parameters (Table 1). In addition, an 80 dBSPL click was used for reference. All the data presented are the average of 150 trials.

All experiments were conducted within the guidelines of the Animal Experiments Committee of the University of Tokyo.

Data analyses: The cortical AEP of a rat has typical fast positive/negative biphasic onset waves (P1/N1) followed by slow biphasic waves (P2/N2), thereby forming the P1-N1-P2-N2 complex. Under particular conditions, this complex is then followed by relatively fast biphasic offset waves (P_{OFF}/N_{OFF}). We first digitally filtered the measured AEP and separated the fast P1/N1 and P_{OFF}/N_{OFF} waves from the slow P2/N2 waves. We routinely used a zero-phase finite impulse response filter with a 129th order and passband of 10–80 Hz. The passband was sometimes readjusted depending on the predominant frequency range of the measured AEP.

We identified the overall characteristics of offset responses by taking the root mean square (RMS) values within 100 ms after the stimulus termination and averaging RMS values across recording sites. This averaged RMS value refers to an offset cortical activity level (CAL) in this work. Likewise, average RMS values within 100 ms after the onset of stimuli and without stimuli were also defined as onset and spontaneous CAL, respectively, and measured for reference. The time range of CAL was changed depending on filter passband.

We obtained the distribution of onset (P1-N1) and offset (P_{OFF}-N_{OFF}) amplitude and estimated the location of local maximum. To pool the peak location across animals, all the peak locations were plotted in the coordinate, in which the locations of the click-evoked P1 maximums were taken as a common origin. We also explored the onset tonotopic representation for reference by extracting the local maximum of P1 of a faint 40 dBSPL tone. This local maximum is expediently called the characteristic frequency (CF) location according to the test frequency. We finally characterized the amplitude and latency of maximally responsive onset and offset potentials as a function of test frequencies.

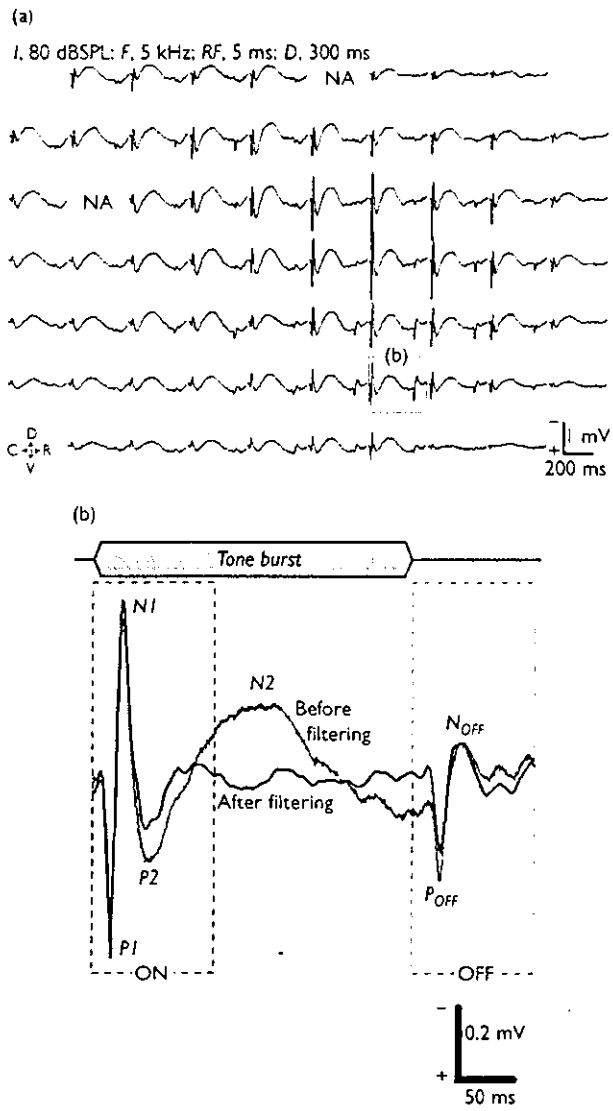

Fig. 1. Experimental data analyzed. (a) Cortical map of tone-burst-evoked potentials. An experimental condition is indicated in each inset here and hereafter. R, rostral; C, caudal; D dorsal; and V, ventral. (b) Definition of the evoked potential waves (P1, N1, P2, N2, P_{OFF}, N_{OFF}) and filtering of the waveform.

RESULTS

Figure 1a shows the typical AEP patterns mapped over the auditory cortex, and Fig. 1b defines the AEP waves (P1, N1, P2, N2, P_{OFF}, and N_{OFF}) and shows how the filtering separated onset and offset components from the measured AEP.

Offset CAL was as low as the spontaneous CAL under 40 and 60 dBSPL, but was significantly higher than the spontaneous CAL under 80 dBSPL (two-side *t*-test here and hereafter for statistical analyses, $p<0.01$), suggesting that distinct offset responses were produced (Fig. 2a,i). Shortening a fall time induced a high offset CAL (20 ms *vs* 1 ms, $p<0.01$). Nevertheless, tones with an intensity of 80 dBSPL and a fall time of 10 ms resulted in a significantly larger offset CAL than tones with 60 dBSPL and 1 ms fall time ($p<0.01$), despite the same decreasing rate. In contrast, onset CAL was generally determined only by the increasing rate of pressure change at a stimulus onset, and CAL at the same increasing rate but different intensities were not statistically significantly different ($p<0.1$). Offset responses

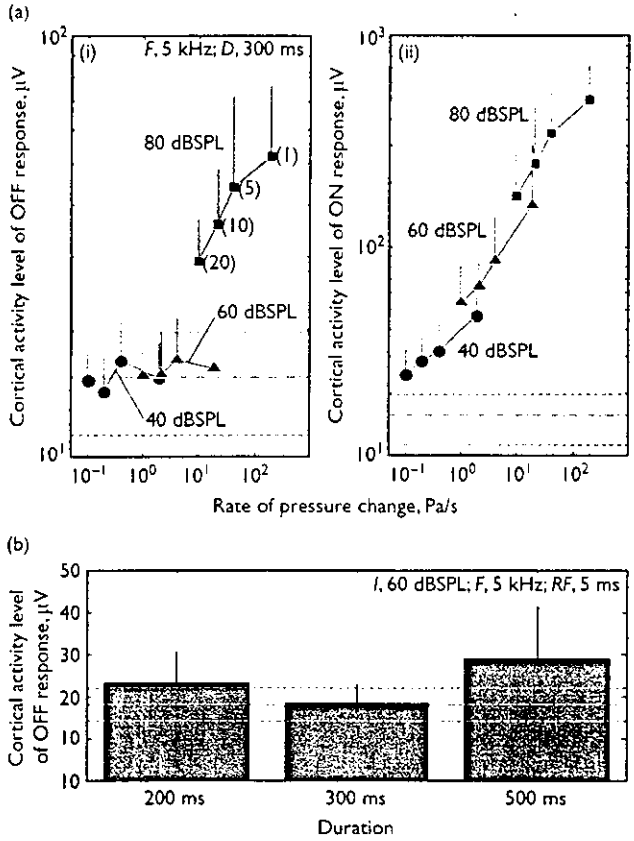

Fig. 2. Cortical activity level. (a) Offset (i) and onset (ii) CAL as a function of rate of pressure change (Pa/s). Digits in parentheses indicate rise-fall times. A bar on each marker indicates s.d. here and hereafter. Dashed and broken lines indicate the mean and s.d. of a spontaneous CAL, respectively. (b) Offset CAL as a function of duration. Because offset responses of 500 ms duration tones contained frequencies lower than 10 Hz, we used a 5–80 Hz filter and obtained 200 ms RMS values for CAL.

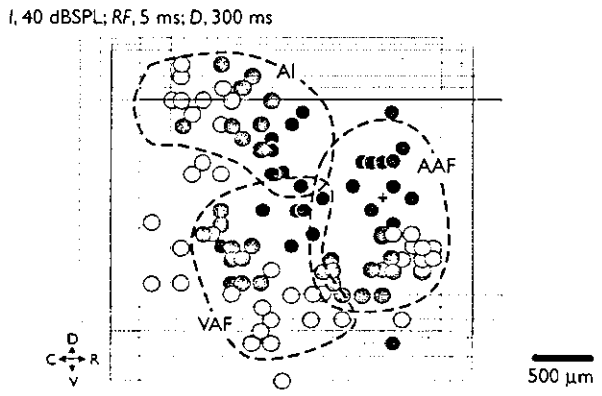

Fig. 3. Tonotopic representation obtained from 12 rat auditory cortices and tonotopicity-based identification of AI, AAF, and VAF. Test frequencies: white, 5 kHz; half tone, 20 kHz; and dark, 40 kHz. PI local maximums of 40 dBSPL tones were plotted with respect to 80-dBSPL-click-evoked PI (+). Squares indicate sensing areas of individual cortices.

were also sensitive to sound duration (Fig. 2b), and long-duration stimuli generally produced large offset responses (e.g. 500 ms duration *vs* 300 ms duration tones, $p<0.05$). However, 200 ms duration tones also evoked larger offset responses than 300 ms duration tones ($p<0.1$), suggesting that offset responses have more complicated duration-tuning characteristics.

AI, AAF and VAF of a rat showed different tonotopic organizations (Fig. 3). AI had a clear posterior-to-anterior tonotopic gradient from low to high frequencies, while AAF and VAF forms a C-shaped tonotopic organization with low- and high-frequencies rostrally and dorsocaudally, respectively. On the other hand, offset responses had a poor tonotopic distribution, but generally appeared at the fringe of their onset responses, resulting in spatial segregation between the onset and offset responses (Fig. 4). Both offset and onset responses appeared over the entire auditory cortex, and the largest responses were usually obtained from AAF. Compared with the tonotopic map (Fig. 3), offset responses were commonly distributed in different CF locations with respect to a test frequency: e.g., the offset responses to 5 kHz tones were elicited in 40 kHz CF location in AI, and 20 kHz CF locations in AAF and VAF.

The amplitude of offset responses (P_{OFF}-N_{OFF}) at a maximally responsive location was sensitive to the test frequencies, and high frequency tones produced large offset responses (5 kHz *vs* 40 kHz, $p<0.01$), while onset responses (P1-N1) were independent of test frequencies (Fig. 5). Likewise, high frequency tones resulted in short latencies in offset responses (P_{OFF}, N_{OFF}; 5 kHz *vs* 40 kHz, $p<0.01$), while no significant difference was observed in onset responses (P1, N1).

DISCUSSION

Tones with high frequency, short fall time, and long duration generally elicited large offset responses. High-frequency selectivity was not reported previously, but this could be species-specific, given that a frequency domain conveying important information is likely different across animals (e.g., ultrasonic communication for rats, sonic communication for human, and specific frequency range for bat echolocation). A similar fall time tuning was found in a human ABR [2], and the duration tuning was also consistent with several animal unit studies from the midbrain [6,11,14] to auditory cortex [15].

Offset responses showed poor tonotopicity and generally appeared at the fringe of their onset responses. Our results directly verified the previous human MEG studies of the auditory cortex, which inferred that the sources of offset responses slightly differed from onset sources [3], and that the high-frequency offset sources were located close to the low-frequency onset sources [4]. Such distributions may be associated with the complementary tuning characteristics of onset and offset responses, which were found by ABR studies [1], and unit studies in the thalamus [13] and cortex [17]; the tuning curves of offset components had two peaks: one at a frequency lower than and the other at a frequency higher than the onset tuning frequency.

Previous patch-clamp recording and pharmacological studies showed evidence that duration-tuned neurons and off neurons probably receive inhibitory inputs prior to the excitation at the stimulus onset and that inhibition is strongest at its onset and is sustained throughout the duration of a sound [7–9]. Taken together with our results, an offset response may be formed by a rebound after an inhibitory input [10,12,19], and the rebound can mainly explain our results as well as previous findings. First, sound

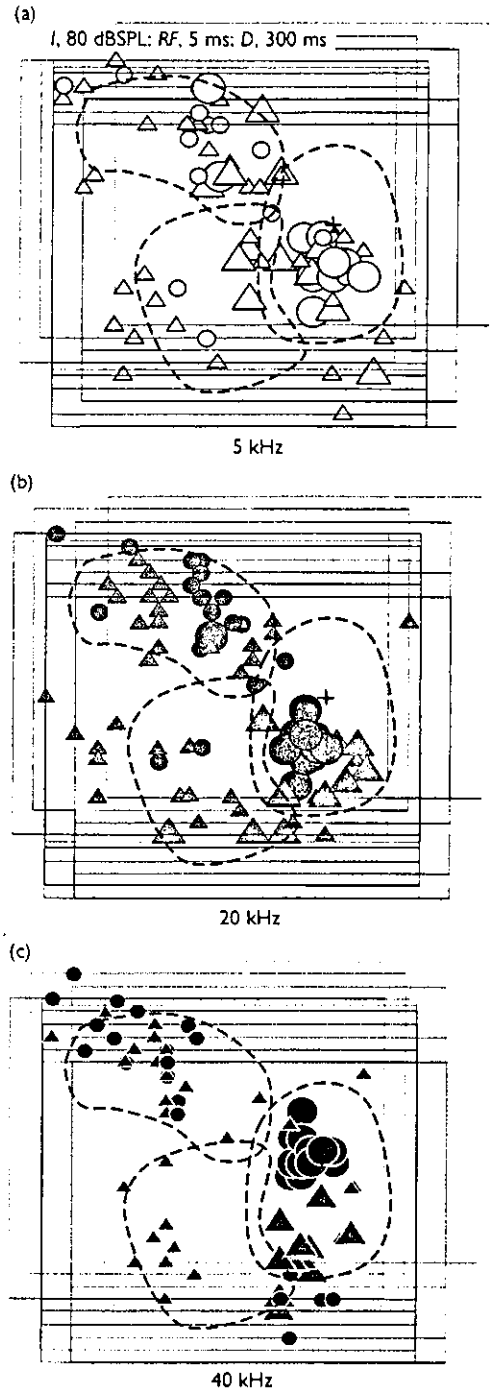

Fig. 4. Local maximums of onset (circles) and offset (triangles) responses recorded from 12 rat auditory cortices. Test frequencies: (a) 5 kHz; (b) 20 kHz; and (c) 40 kHz. Large symbols indicate the maximally responsive locations. See Fig. 3 for the presentation conventions.

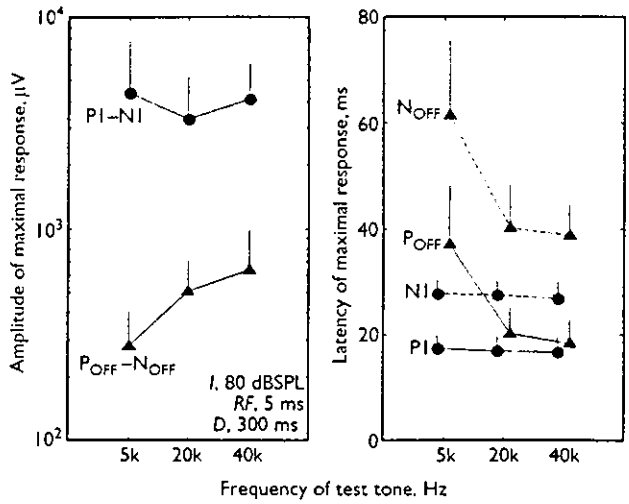

Fig. 5. Amplitude and latency of maximal onset (circles) and offset (triangles) responses as a function of test frequency.

intensity and duration may have relevance to inhibitory strength and period, thereby causing a stronger resumption when intensity and duration increase. Second, a short fall time may make the rebound more synchronous, thereby enhancing responses. Third, the spatial patterns of onset and offset responses may reflect the excitatory and inhibitory response areas of the common tune curves of cortical neurons, in which the inhibitory response areas, known as inhibitory sidebands, usually flank the excitatory response areas [19]. The extrinsic optical recording in the guinea pig auditory cortex also demonstrated that the excitatory response areas were sandwiched or surrounded by inhibitory areas [20], and this may explain the poor tonotopicity of offset responses.

The dominant recruitment of inhibition and the complicated interaction of excitatory inputs could endow offset responses with more ambiguous characteristics than onset responses. Difference in binaurality, amplitude, or spectral bandwidth can influence the temporal interaction [8,10] and the integration of this interaction can induce context-dependent changes in the response properties of neurons. Many neurons commonly show changes in their general duration-tuning characteristics and sometimes their response type (i.e., on, on/off, and off), depending on sound intensity, stimulus repetition rate, and stimulus type [11,13,14,16].

CONCLUSION

The present study characterized the auditory-evoked offset responses of the rat auditory cortices by multiple-site surface microelectrode recording. Offset responses were facilitated when the intensity of test tones was high, the fall time was short, and the duration was long. Offset responses did not appear tonotopically, but at the fringe of tonotopic onset distributions. A rebound after the inhibition in the presence of a stimulus may best explain our results, and yet some complicated interactions with other inputs should be taken into account for a unified view of duration-tuned offset responses.

REFERENCES

1. Henry KR. Tuning of the auditory brain stem OFF response is complementary tuning of the auditory brain stem ON response. *Hear Res* 1985; 19:115–125.

2. Van Campen LE, Hall III JW and Grantham DW. Human offset auditory brainstem response: effects of stimulus acoustic ringing and rise-fall time. *Hear Res* 1997; 103:35–46.
3. Hari R, Pelizzone M, Makela JP, Hallstrom J, Leinonen L and Lounasmaa OV. Neuromagnetic responses of the human auditory cortex to on- and offsets of noise bursts. *Audiology* 1987; 26:31–43.
4. Noda K, Tonoike M, Doi K, Koizuka I, Yamaguchi M, Seo R *et al.* Auditory evoked off-response: its source distribution is different from that of on-response. *Neuroreport* 1998; 9:2621–2625.
5. Suga N and Manabe T. Neural basis of amplitude-spectrum representation in auditory cortex of the mustached bat. *J Neurophysiol* 1982; 47:225–255.
6. Gooler DM and Feng AS. Temporal coding in the frog auditory midbrain: the influence of duration and rise-fall time on the processing of complex amplitude-modulated stimuli. *J Neurophysiol* 1992; 67:1–22.
7. Casseday JH, Ehrlich D and Covey E. Neural measurement of sound duration: control by excitatory-inhibitory interactions in the inferior colliculus. *J Neurophysiol* 2000; 84:1475–1487.
8. Covey E, Kauer JA and Casseday JH. Whole-cell patch clamp recording reveals subthreshold sound-evoked postsynaptic current in the inferior colliculus of awake bats. *J Neurosci* 1996; 16: 3009–3018.
9. Fuzessery ZM and Hall JC. Sound duration selectivity in the pallid bat inferior colliculus. *Hear Res* 1999; 137:137–154.
10. Kuwada S and Batra R. Coding of sound envelops by inhibitory rebound in neurons of the superior olivary complex in the unanesthetized rabbit. *J Neurosci* 1999; 19:2273–2287.
11. Brand A, Urban A and Grothe B. Duration tuning in the mouse auditory midbrain. *J Neurophysiol* 2000; 84:1790–1799.
12. Calford MB and Webster WR. Auditory representation within principal division of cat medial geniculate body: and electrophysiological study. *J Neurophysiol* 1981; 45:1013–1028.
13. He J. ON and OFF pathways segregated at the auditory thalamus of the guinea pig. *J Neurosci* 2001; 21:8672–8679.
14. He J. OFF responses in the auditory thalamus of the guinea pig. *J Neurophysiol* 2002; 88:2377–2386.
15. He J, Hashikawa T, Ojima H and Kinouchi Y. Temporal integration and duration tuning in the dorsal zone of cat auditory cortex. *J Neurosci* 1997; 17:2615–2625.
16. Galazyuk AV and Feng AS. Encoding of sound duration by neurons in the auditory cortex of the little brown bat, *Myotis lucifugus*. *J Comp Physiol A* 1997; 180:301–311.
17. Pelleg-Toiba R and Wollberg Z. Tuning properties of auditory cortex cells in the awake squirrel monkey. *Exp Brain Res* 1989; 74:353–364.
18. Takahashi H, Ejiri T, Nakao M, Nakamura N, Kaga K and Herve T. Microelectrode array on folding polyimide ribbon for epidural mapping of functional evoked potentials. *IEEE Trans Biomed Eng* 2003; 50:510–516.
19. Phillips DP, Hall SE and Boehnke SE. Central auditory onset response, and temporal asymmetries in auditory perception. *Hear Res* 2002; 167:192–205.
20. Horikawa J, Hosokawa Y, Kubota M, Nasu M and Taniguchi I. Optical imaging of spatiotemporal patterns of glutamatergic excitation and GABAergic inhibition in the guinea-pig auditory cortex *in vivo*. *J Physiol* 1996; 497:629–638.

Acknowledgements: We are grateful to Mr. T. Ejiri, Mr. F. Mase, Mr. T. Ota, and Dr. S.A. Schmerber for their dedicated support in the experiments.

Available online at www.sciencedirect.com
SCIENCE DIRECT
Hearing Research 190 (2004) 161–168
HEARING RESEARCH
www.elsevier.com/locate/heares

Vestibular-evoked myogenic potentials in three patients with large vestibular aqueduct

Kianoush Sheykholeslami *, Sébastien Schmerber, Mohammad Habiby Kermany, Kimitaka Kaga

Department of Otolaryngology, Faculty of Medicine, University of Tokyo, 7-3-1, Hongo, Bunkyo-Ku, Tokyo 113-0033, Japan

Abstract

An enlarged vestibular aqueduct (LVA) is a common congenital inner ear anomaly responsible for some unusual vestibular and audiological symptoms. Most of the cases show bilateral early onset and progressive hearing loss in children. The gross appearance on CT scan of the inner ear is generally normal. However, precise measurements of the inner ear components reveal abnormal dimensions, which may account for the accompanying auditory and vestibular dysfunction. Despite extensive studies on hearing and the vestibular apparatus, saccular function is not studied. To our knowledge this is the first report of saccular malfunction in three patients with LVA by means of vestibular evoked myogenic potentials. Conventional audiograms revealed bilateral severe sensorineural hearing loss in two patients and mixed type hearing loss in one patient. Two of the patients complained about vertigo and dizziness but vestibular assessments of the patients showed normal results. The diagnosis had been made by high-resolution CT scans and MR images of the skull that showed LVA in the absence of other anomalies. The VEMP threshold measured from the ear with LVA in two patients with unilateral enlargement of the vestibular aqueduct was 75–80 dB nHL whereas the threshold from normal ears was 95 dB nHL. The third patient with mixed type hearing loss and bilateral LVA had VEMP responses despite a big air–bone gap in the low frequency range. The VEMP in this patient was greater in amplitude and lower in threshold in the operated ear (the patient had a tympanoplasty which did not improve her hearing). These findings and results of other patients with Tullio phenomenon and superior semicircular canal dehiscence, who also showed lower VEMP threshold, confirmed the theory of a 'third window' that allows volume and pressure displacements, and thus larger deflection of the vestibular sensors, which would cause the vestibular organ to be more responsive to sound and pressure changes.

Key words: Large vestibular aqueduct; Vestibular-evoked myogenic potential; Vestibular; Myogenic potential; Sacculus end-organ hypersensitivity; Vestibulocollic reflex

1. Introduction

Although the vestibular end-organs are primarily responsive to head movement and acceleration, non-physiological stimuli, including sound, have been shown to be capable of activating populations of vestibular afferents. Behavioral and physiological studies indicate that the sacculus functions in part as a hearing organ in several non-mammalian species (fish, Popper and Fay, 1973; rays, Löwenstein and Roberts, 1951; toads, Moffat and Capranica, 1976; and birds, Wit et al., 1984) as well as in mammals. For example, sensitivity of the sacculus to sound has been demonstrated among mammals, including guinea pigs (Cazals et al., 1983), cats (MacCue and Guinan, 1995), and squirrel monkeys (Young et al., 1977). In humans, intense sound and vibration can produce vestibular reflexes and illusions of movement (Von Békésy, 1935; Lackner and Graybeil, 1974; Parker et al., 1975). Evidence of this kind suggests that the mammalian sacculus has retained sensitivity to sound. In a series of reports, Bickford et al. (1964) reported an 'inion response' to loud sound and

* Corresponding author. Present address: Department of Neurobiology and Pharmacology, Northeastern Ohio Universities College of Medicine, 4209 State Route 44, P.O. Box 95, Rootstown, OH 44272-0095, USA. Fax: +1 (330) 325-55916.
E-mail address: ksheykho@neoucom.edu (K. Sheykholeslami).

Abbreviations: LVA, large vestibular aqueduct; LVAS, large vestibular aqueduct syndrome; VA, vestibular aqueduct; VEMP, vestibular-evoked myogenic potential; SCM, sternocleidomastoid muscle; STB, short tone burst

0378-5955/04/$ - see front matter © 2004 Published by Elsevier B.V.
doi:10.1016/S0378-5955(04)00018-8